Timing jitter of ultrashort solitons in high-speed communication systems. I. General formulation and application to dispersion-decreasing fibers

René-Jean Essiambre* and Govind P. Agrawal†

The Institute of Optics and Rochester Theory Center for Optical Science and Engineering, University of Rochester, Rochester, New York 14627

Received March 5, 1996; revised manuscript received July 17, 1996

By using adiabatic perturbation theory, we calculate the timing jitter generated by fluctuations in soliton amplitude, frequency, and position that are induced by the amplifiers noise in high-speed soliton communication systems. The analysis is applied to dispersion-tailored fibers which, in contrast with conventional constant-dispersion fibers, allow ultrashort solitons (width < 10 ps) to propagate over long distances with minimum production of dispersive waves. We show that a transition from a regime in which amplifier noise-induced frequency fluctuations dominate the timing jitter (Gordon–Haus jitter) to a regime in which amplitude fluctuations dominate the timing jitter occurs when solitons become shorter than 2–7 ps, depending on the total distance of transmission. The latter source of jitter arises because fluctuations in the soliton amplitude are converted to frequency fluctuations by the Raman effect, which in turn are converted to position fluctuations by the group-velocity dispersion. The contribution of third-order dispersion to the timing jitter is evaluated and discussed. We provide an estimate of the distance at which soliton-control elements (such as synchronous modulators) should be inserted to reduce the timing jitter and extend the transmission distance. © 1997 Optical Society of America [S0740-3224(97)01802-X]

Key words: Amplifier noise, solitons, optical fiber communication, nonlinear optics, optical fiber dispersion.

1. INTRODUCTION

Since the first demonstration of soliton transmission over long distances,[1] optical solitons have been thought of as natural bits of information for fiber-optic communications. Any soliton train must be amplified for compensating the fiber loss to ensure its stable propagation over long distances. For the lumped-amplification scheme, implemented commonly by use of erbium-doped fiber amplifiers, the amplifier spacing must be smaller than the soliton period to allow solitons to propagate down a fiber link with minimal generation of dispersive waves.[2] This condition imposes a lower limit on the soliton duration (~10 ps) and consequently an upper limit on the bit rate (~20 Gb/s) for typical amplifier spacings (~30 km). Within this so-called average-soliton regime the timing jitter due to frequency fluctuations induced by the amplifiers noise (spontaneous emission) limits the total transmission distance at relatively low bit rates (<10 Gb/s) to lengths of ~5000 km (the Gordon–Haus limit[3]). However, the use of some form of soliton control, such as sliding-frequency filters[4] or synchronous modulation,[5] has been shown to allow nearly error-free operation (bit-error rate less than 10^{-9}) beyond the Gordon–Haus limit. In essence, the use of soliton-control mechanisms allows soliton communication systems to operate at bit rates close to the limit imposed by the average-soliton regime.

For an increase in the bit rate of soliton communication systems beyond 20 Gb/s, alternative schemes must be developed. Two different approaches are currently being considered. One scheme would combine multiple channels using wavelength-division multiplexing, with each channel operating in the average-soliton regime,[6] while the second would pack ultrashort solitons to create a high-speed, time-division-multiplexed bit stream. For practical amplifier spacings the latter approach requires soliton transmission beyond the average-soliton regime. In one attempt to overcome the limits imposed by the average-soliton regime it has been shown[7–9] that solitons of 2–5 ps can be stably transmitted over many soliton periods if a fast-saturable-absorber-type element is present in the line. However, so far, this approach has been limited to moderate amplifier spacings (~20 km). In an alternative novel approach, practically undistorted propagation of ultrashort solitons with large amplifier spacings can be achieved by especially designed fibers with a tailored-dispersion profile.[10] Such fibers allow stable propagation of ultrashort solitons with amplifier spacings as large as 50–100 km.

An important issue, critical for the feasibility of an ultrahigh bit-rate communication system, composed of a chain of amplifiers (see Fig. 1) connecting segments of dispersion-decreasing fibers (DDF's), involves the timing jitter associated with the propagation of ultrashort solitons corrupted by the amplifier noise. Previous analyses on this issue[11,12] have considered the contribution of the Raman effect to the timing jitter in the context of constant-dispersion fibers. However, these analyses were implicitly limited both to the average-soliton regime

0740-3224/97/020314-09$10.00

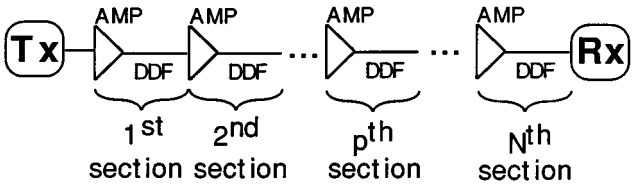

Fig. 1. Schematic representation of a DDF-based fiber link with multiple amplification sections. Tx, transmitter; Rx, receiver.

and to small Raman-induced frequency shifts. Operation in the average-soliton regime with ultrashort solitons requires amplifier spacings below one kilometer and is of limited practical interest for long-haul communication systems. The limitation to small Raman-induced frequency shifts arises because large frequency shifts generally result in pulse distortions and unstable soliton propagation. These deleterious instabilities originate from the combined effect of the Raman-induced frequency shift and the third-order dispersion (TOD) that manifests through a local change of the effective group-velocity dispersion (GVD) along the soliton path and leads to significant emission of dispersive waves. The TOD has been neglected in previous work.[11,12]

In this paper we derive an analytic expression for the timing jitter of ultrashort solitons by including explicitly the contributions of the GVD, the Raman effect, and the TOD, in both custom-tailored DDF's (which can support large Raman-induced frequency shifts[10]) and constant-dispersion fibers. The paper is divided into several sections. Derivation of the trajectory of ultrashort solitons by adiabatic perturbation theory is presented in Section 2. The results are used in Section 3 to evaluate the timing jitter at the output of a chain of amplifiers connecting multiple identical DDF segments (see Fig. 1). Section 4 presents the results and discusses the relative contributions of different physical origins to the timing jitter. In Part II of this paper we consider the use of periodic optical phase conjugation of the soliton train for reducing the timing jitter and discuss the use of bandpass filters and the role played by dispersion fluctuations.

2. ADIABATIC PERTURBATION THEORY

The propagation of ultrashort solitons through a DDF is described by a generalized nonlinear Schrödinger equation[13]:

$$i\frac{\partial u}{\partial z}+\frac{1}{2}p(z)\frac{\partial^2 u}{\partial \tau^2}+|u|^2u=-i\frac{\alpha}{2}u+\tau_R u\frac{\partial |u|^2}{\partial \tau}+i\delta_d\frac{\partial^3 u}{\partial \tau^3}, \tag{1}$$

where $p(z)=|\beta_2(z)/\beta_2(0)|$ is the normalized GVD, α is the fiber loss, $\delta_d=\beta_3/[6T_0|\beta_2(0)|]$ is the normalized TOD, and τ_R governs intrapulse Raman scattering.[13] Note that Eq. (1) is written in soliton units and the GVD $\beta_2(0)$ used for normalization corresponds to the GVD at the input end of a DDF segment. Thus time τ is normalized to the soliton characteristic width T_0, and distance z is normalized to the dispersion length $L_D=T_0^2/|\beta_2(0)|$. The soliton width (full width at half-maximum) T_s is related to T_0 by $T_s\simeq 1.763T_0$. The use of Eq. (1) for describing soliton evolution implies that polarization effects are ignored in the following analysis.

In order to apply the adiabatic perturbation theory[14,15] (APT), we rescale the normalized field u and distance z in Eq. (1) to a new amplitude v and a new distance scale η, defined by the following relations:

$$v=p^{-1/2}u, \tag{2}$$

$$\eta=\int_0^z p(y)dy. \tag{3}$$

These transformations are, in fact, renormalizations of the soliton amplitude and the distance scale to the local GVD and dispersion length. In terms of v and η, Eq. (1) becomes

$$i\frac{\partial v}{\partial \eta}+\frac{1}{2}\frac{\partial^2 v}{\partial \tau^2}+|v|^2v=-i\left(\frac{\alpha}{2p}+\frac{1}{2p}\frac{\mathrm{d}p}{\mathrm{d}\eta}\right)v+\tau_R v\frac{\partial |v|^2}{\partial \tau}+i\frac{\delta_d}{p}\frac{\partial^3 v}{\partial \tau^3}. \tag{4}$$

The left side of Eq. (4) corresponds to the standard nonlinear Schrödinger equation.

For relatively wide solitons ($T_s>10$ ps) the effects of higher-order nonlinear and dispersive effects, governed by the last two terms of Eq. (4), are negligible. If the dispersion profile of DDF matches the power loss,

$$p(z)=\exp(-\alpha z), \tag{5}$$

then the first term on the right side of Eq. (4) also vanishes. Thus in a DDF whose dispersion decreases exponentially, relatively wide solitons ($T_s>10$ ps) can propagate undistorted in spite of fiber loss. Such a soliton communication system with periodic amplification can transmit data over long distances with relatively long amplifier spacings (80–100 km), limited only by the realizable minimum dispersion $\beta_2^{\min}$ at the end of each DDF section.[10]

For high-speed soliton communication systems the soliton width must be reduced to <5 ps as the bit rate increases. The higher-order effects [the last two terms of Eq. (4)] cannot be neglected for such short solitons. The Raman term (governed by τ_R) can be treated as a small perturbation for the soliton widths considered here (>1 ps). As verified numerically, TOD (the last term) is also a small perturbation for $|\beta_2^{\min}|$ larger than ~ 0.1 ps^2/km. The minimal dispersion $\beta_2^{\min}\equiv\beta_2(z_a)$ is the GVD at the DDF end, where z_a is the normalized amplifier spacing.

We now apply the APT[14,15] to Eq. (4) by taking its unperturbed solution as a fundamental soliton of the form

$$v_s(B,q,\phi,\omega;\tau)=B\ \mathrm{sech}[B(\tau-q)]\exp(i\phi-i\omega\tau), \tag{6}$$

where the parameters B, q, ϕ, and ω represent the amplitude, position, phase, and frequency of the rescaled soliton, respectively, and are slowly varying functions of the rescaled distance η. If we treat the three terms on the

right side of Eq. (4) as a small perturbation written as $\epsilon P[v_s]$, where ϵ is a small parameter, the evolution of the soliton parameters is governed by[16]

$$\frac{dB}{d\eta} = \mathrm{Im}\int_{-\infty}^{\infty} \epsilon P[v_s] U_B d\tau, \tag{7}$$

$$\frac{d\omega}{d\eta} = \mathrm{Re}\int_{-\infty}^{\infty} \epsilon P[v_s] U_\omega d\tau, \tag{8}$$

$$\frac{dq}{d\eta} = -\omega + \frac{1}{B}\,\mathrm{Im}\int_{-\infty}^{\infty} \epsilon P[v_s] U_q d\tau, \tag{9}$$

$$\frac{d\phi}{d\eta} = q\,\frac{d\omega}{d\eta} + \frac{B^2-\omega^2}{2} - \frac{1}{B}\,\mathrm{Re}\int_{-\infty}^{\infty} \epsilon P[v_s] U_\phi d\tau, \tag{10}$$

where Im stands for imaginary part, and the set of functions over which the perturbation is projected is given by

$$U_B = v_s^*, \tag{11}$$

$$U_\omega = \tanh[B(\tau-q)]v_s^*, \tag{12}$$

$$U_q = (\tau-q)v_s^*, \tag{13}$$

$$U_\phi = \{1 - B(\tau-q)\tanh[B(\tau-q)]\}v_s^*. \tag{14}$$

The evolution equations for the soliton parameters B, ω, q, and ϕ for a DDF are obtained by replacing $\epsilon P[v_s]$ in Eqs. (7)–(10) by the terms on the right side of Eq. (4). The integration over τ is cumbersome but straightforward and leads to the following simple equations:

$$\frac{dB}{d\eta} = -\left(\frac{\alpha}{p} + \frac{1}{p}\frac{dp}{d\eta}\right)B, \tag{15}$$

$$\frac{d\omega}{d\eta} = -\frac{8}{15}\,\tau_R B^4, \tag{16}$$

$$\frac{dq}{d\eta} = -\omega + \frac{\delta_d}{p}\,(B^2 + 3\omega^2). \tag{17}$$

We omit here the evolution equation of $\phi(\eta)$ because the timing jitter does not depend on the soliton phase when soliton interaction is negligible. Solitons are assumed to be sufficiently far apart that we can neglect the contribution of soliton interaction to the timing jitter. It is interesting to note that, within the framework of APT, intrapulse Raman scattering affects only the soliton frequency [see Eq. (16)] while TOD affects only the soliton position [see Eq. (17)]. However, since the frequency ω appears in Eq. (17), the Raman effect indirectly affects the soliton position as well. Before integrating Eqs. (15)–(17), it is useful to rewrite them in terms of the unscaled variables u and z (see Appendix A). The functional form of u_s is the same as the rescaled soliton v_s, as evident by Eq. (2): The two differ only by their different amplitudes, related by $A = Bp^{1/2}$. The evolution of the normalized amplitude A is easily obtained by Eq. (15), after use of Eqs. (2) and (3), and is given by

$$A(z) = A_0\,\frac{\exp(-\alpha z)}{\sqrt{p(z)}}. \tag{18}$$

For an ideal loss-matched dispersion profile, [$p(z) = \exp(-\alpha z)$], the amplitude decreases as $A(z) = A_0\exp(-\alpha z/2)$, as expected from simple energy-loss considerations. Moreover, the soliton width stays constant over the entire DDF length for such an ideal profile. Equation (18) is, however, valid even for nonexponential profiles.

We now assume a DDF with an ideal loss-matched dispersion profile (effects of deviations from the ideal profile are discussed in Part II). Its use allows us to solve Eqs. (15)–(17) exactly and obtain the evolution of the soliton amplitude, frequency, and position along the fiber in the form

$$A(z) = A_0\exp(-\alpha z/2), \tag{19}$$

$$\omega(z) = -\frac{8}{15}\,\tau_R z_1(z) A_0^4 + \omega_0, \tag{20}$$

$$q(z) = q_{\mathrm{GH}}(z)\omega_0 + q_R(z)A_0^4 + q_{\mathrm{TOD}}^A(z)A_0^2 + q_{\mathrm{TOD}}^\omega(z)\omega_0^2 + q_{\mathrm{C1}}(z)A_0^8 + q_{\mathrm{C2}}(z)A_0^4\omega_0 + q_0. \tag{21}$$

A_0, ω_0, and q_0 are the initial values (at the front end of the fiber located at $z = 0$) of the soliton amplitude, frequency, and position, respectively:

$$q_{\mathrm{GH}}(z) = -z_1(z), \qquad q_R(z) = \frac{8}{15}\,\frac{\tau_R}{\alpha}\,[z_1(z) - z_2(z)], \tag{22}$$

$$q_{\mathrm{TOD}}^A(z) = \delta_d z, \qquad q_{\mathrm{TOD}}^\omega(z) = 3\delta_d z, \tag{23}$$

$$q_{\mathrm{C1}}(z) = \frac{64}{75}\,\frac{\delta_d \tau_R^2}{\alpha^2}\,[z - 2z_1(z) + z_2(z)],$$

$$q_{\mathrm{C2}}(z) = -\frac{16}{5}\,\frac{\delta_d \tau_R}{\alpha}\,[z - z_1(z)], \tag{24}$$

$$z_1(z) = [1 - \exp(-\alpha z)]/\alpha,$$

$$z_2(z) = [1 - \exp(-2\alpha z)]/(2\alpha), \tag{25}$$

where the parameters $z_1(z)$ and $z_2(z)$ are introduced for convenience. The term $q_{\mathrm{GH}}(z)$ leads to the Gordon–Haus effect in DDF's. The term $q_R(z)$ is associated with the displacement of the soliton position due to the intrapulse Raman effect alone. The two terms $q_{\mathrm{TOD}}^A(z)$ and $q_{\mathrm{TOD}}^\omega(z)$ govern the effects of TOD on the soliton position. The last two terms, $q_{\mathrm{C1}}(z)$ and $q_{\mathrm{C2}}(z)$, represent cross effects between TOD and the Raman effect and are often small because of the product $\delta_d\tau_R$ appearing in them.

Full numerical simulations of Eq. (1) for various parameter combinations have shown that Eq. (21) predicts the evolution of soliton position over one amplification section with an accuracy better than 1% of the total time shift for nearly all values of the parameters used in this paper. To illustrate this, Fig. 2 shows (open circles) the difference in the soliton position $q(z_a)$ at the end of one DDF between the value predicted from Eq. (21) and the value obtained by solving numerically Eq. (1). The parameters of the DDF are $\beta_2^{\min} = -0.2$ ps^2/km, $\alpha = 0.22$ dB/km, $\beta_3 = 0.07$ ps^3/km, $T_R = 6$ fs, and a fiber length of

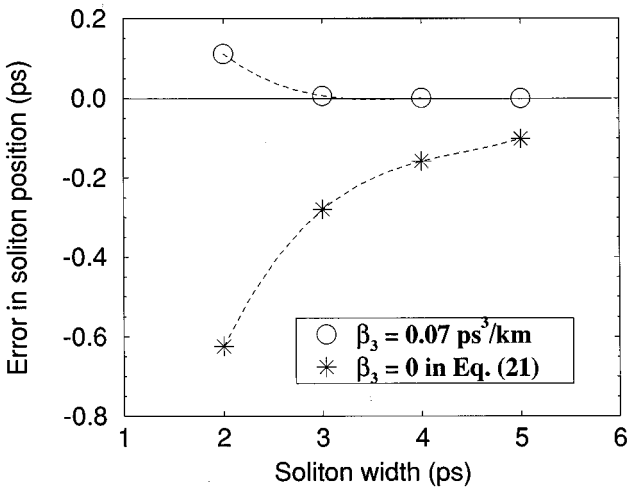

Fig. 2. Estimation of the accuracy of the APT over one stage and the relative importance of β_3. Open circles represent the difference between the soliton position obtained from the APT and the value obtained by solving Eq. (1) numerically. Stars represent the same difference, but β_3 is neglected in the APT.

70 km. The difference in the soliton position is < 1 fs for $T_s = 5$ ps and increases gradually to become 120 fs when $T_s = 2$ ps. The total shift in the soliton position resulting from higher-order effects (Raman and TOD) was 17.8 ps for the 2-ps soliton so that the APT and numerical results agree within 1%. If we neglect β_3 in Eq. (21) (but keep it in the numerical simulation), the two disagree by more than 5% (stars), indicating the importance of keeping the β_3 term in the APT. Note, however, that for a large number of cascaded sections the accuracy of the APT will degrade, especially for low $|\beta_2^{\min}|$, because of accumulation of dispersive waves. Further details are given in Section 4 of Part I and Section 3 of Part II of this paper.

We can carry out a similar analysis for the soliton trajectory for the case of a constant-dispersion fiber by using Eq. (1) with $p(z) = 1$ and neglecting losses (which are assumed to be compensated periodically as in the average-soliton regime). The soliton amplitude $A(z)$ now represents the average amplitude of the soliton over one section and is consequently a constant A_0. The frequency shift is as previously derived in Ref. 17. The calculation of the soliton trajectory leads to an equation of the same form as Eq. (21) but with different coefficients, given by

$$q_{\mathrm{GH}}(z) = -z, \quad q_R(z) = \frac{4}{15}\,\tau_R z^2,$$

$$q_{\mathrm{TOD}}^{A}(z) = \delta_d z, \quad q_{\mathrm{TOD}}^{\omega}(z) = 3\,\delta_d z,$$

$$q_{\mathrm{C1}}(z) = \frac{64}{225}\,\delta_d \tau_R^2 z^3,$$

$$q_{\mathrm{C2}}(z) = -\frac{8}{5}\,\delta_d \tau_R z^2. \tag{26}$$

It is important to discuss the range of validity of the APT. Previous analyses[11,12] have derived the Raman-induced timing jitter in constant-dispersion fibers by essentially using the two terms q_{GH} and q_R in Eq. (21) but without taking into account four additional terms introduced by the TOD. The APT used in the previous analyses[11,12] also assumes that the pulse is a soliton perturbed by the Raman effect. However, when an ultrashort soliton travels in a fiber, the combined effect of the Raman-induced frequency shift and TOD changes the effective GVD experienced by the soliton. In fact, for ultrashort solitons the effective local dispersion in a constant-dispersion fiber can be quite different from the dispersion experienced at the fiber input. We numerically observed that this change of effective local GVD often results in the destruction of the soliton (pulse splitting, considerable emission of dispersive waves, etc.) after propagation over relatively short distances of ~40–50 km. In some cases in which TOD appears to be initially advantageous because of pulse compression, the cumulative frequency shift eventually changes the soliton evolution to the extent that it leads to the destruction of the soliton after several amplification sections.

Realizing that soliton stability is of primary importance for soliton-based communication systems, we find the use of DDF's essential when ultrashort solitons must be used. In fact, for solitons shorter than 0.5–2 ps (depending on the fiber length and the dispersion profile), the DDF's must be especially designed to prevent the soliton from being destroyed by the mutual interaction of higher-order effects. In the analysis performed here the use of APT is equivalent to implicitly assuming that the GVD profile of each DDF is properly tailored to compensate for the higher-order effects as described in Ref. 10. For such fiber designs the average dispersion felt by the soliton is loss matched. Another implicit assumption underlying the application of APT in determining the timing jitter over many amplifier spacings is that the soliton integrity is preserved in all fibers composing the link. Our numerical simulations with solitons of width >3 ps show that, in the absence of soliton control, instabilities generally appear before the Raman-induced timing jitter becomes of concern because of the change of GVD with the accumulated frequency downshift from fiber to fiber. In the following timing-jitter calculations, we shall not take into account explicitly this frequency-shift accumulation, but assume that a compensation scheme is used. This compensation mechanism could be, for example, bandpass filters or synchronous modulators (for limited soliton-frequency shifts). An example of timing-jitter reduction achieved with the compensation of the soliton-frequency shift (and not limited to small shifts) is given in Part II of this paper.

3. TIMING JITTER FOR DISPERSION-DECREASING FIBERS

Returning to the calculation of the timing jitter, we first consider an isolated section of the DDF link (see Fig. 1) and evaluate the time shift $\delta q(z_a)$ at the end of this DDF section because of fluctuations in the soliton amplitude, mean frequency, and position induced by the noise added by the amplifier of this section only. If δA_0, $\delta\omega_0$, and δq_0 represent such fluctuations, $\delta q(z_a)$ is obtained by differentiating Eq. (21) and substituting $z = z_a$ in the resulting expression:

$$\delta q(z_a) = q_{\mathrm{GH}}(z_a)\delta\omega_0 + 4q_R(z_a)A_0^3\delta A_0 + 2q_{\mathrm{TOD}}^A(z_a)A_0\delta A_0 + q_{\mathrm{C2}}(z_a)A_0^4\delta\omega_0 + 8q_{\mathrm{C1}}(z_a)A_0^7\delta A_0 + \delta q_0. \quad (27)$$

In Eq. (27) the two terms $2q_{\mathrm{TOD}}^{\omega}(z_a)\omega_0\delta\omega_0$ and $4q_{\mathrm{C2}}(z_a)\omega_0A_0^3\delta A_0$ obtained from Eq. (21) are omitted because, to first order, the average soliton frequency (in the absence of the Raman effect) ω_0 is zero.

Equation (27) gives the time shift after propagation over one section when only the spontaneous emission of one amplifier is considered (see Fig. 1). However, it is important to note that fluctuations that occurred on previous sections also contribute to the soliton displacement occurring at subsequent sections. Frequency fluctuations are especially important since a change in the soliton mean frequency at a given section will result in a time shift accumulated over all the subsequent sections caused by this frequency shift only. Moreover, because a single amplitude fluctuation at a given section generates not only a frequency fluctuation (because of the Raman effect) at that section but also continues to generate new frequency fluctuations all along the subsequent sections, the timing jitter generated by amplitude fluctuations increases rapidly with the number of sections. The displacement of a soliton at the end of the link composed of N sections, obtained by including all the contributions coming from previous amplifiers, is given by (see Appendix A for more details)

$$\delta q_N = q_{\mathrm{GH}}\sum_{p=1}^{N}\sum_{i=1}^{p}\delta\omega_i + 4q_RA_0^3\sum_{p=1}^{N}\sum_{i=1}^{p}\sum_{j=1}^{i}\delta A_j + 2q_{\mathrm{TOD}}^AA_0\sum_{p=1}^{N}\sum_{i=1}^{p}\delta A_i + q_{\mathrm{C2}}A_0^4\sum_{p=1}^{N}\sum_{m=1}^{p}\sum_{i=1}^{p}\delta\omega_i + 8q_{\mathrm{C1}}A_0^7\sum_{p=1}^{N}\sum_{m=1}^{p}\sum_{i=1}^{p}\sum_{j=1}^{i}\delta A_j + \sum_{p=1}^{N}\delta q_p, \quad (28)$$

where it is understood that all q coefficients are evaluated at $z = z_a$ by use of Eqs. (22)–(25) for DDF's or Eqs. (26) for constant-dispersion fibers. The average displacement $\langle\delta q_N\rangle = 0$ since $\langle\delta\omega_i\rangle = \langle\delta A_i\rangle = \langle\delta q_i\rangle = 0$. The root-mean-square (rms) jitter $\sigma_q \equiv \langle[\delta q_N]^2\rangle^{1/2}$ is obtained by averaging over fluctuations $\delta\omega_i$, δA_i, and δq_i, and its square is given by

$$\sigma_q^2 = \left(\frac{N^3}{3}q_{\mathrm{GH}}^2 + \frac{5}{12}N^4q_{\mathrm{GH}}q_{\mathrm{C2}}A_0^4 + \frac{2}{15}N^5q_{\mathrm{C2}}^2A_0^8\right)\sigma_\omega^2 + \left[2N^4q_Rq_{\mathrm{TOD}}^AA_0^4 + \frac{4}{5}N^5q_R^2A_0^6 + \frac{104}{45}N^6q_Rq_{\mathrm{C1}}A_0^{10} + \frac{4}{3}N^3(q_{\mathrm{TOD}}^A)^2A_0^2 + \frac{44}{15}N^5q_{\mathrm{TOD}}^Aq_{\mathrm{C1}}A_0^8 + \frac{176}{105}N^7q_{\mathrm{C1}}^2A_0^{14}\right]\sigma_A^2 + N\sigma_q^2, \quad (29)$$

where summations over p were replaced by integrals by assuming $N \gg 1$ and it was assumed that the noise of different amplifiers and fluctuations of different soliton parameters are uncorrelated. The quantities σ_A, σ_ω, and σ_q are defined by $\sigma_P \equiv \langle[\delta P]^2\rangle^{1/2}$, where σ_P is the rms deviation of the variable P.

Equation (29) is the main analytical result of this paper. It includes not only the Gordon–Haus jitter (first term on right-hand side) but also the contributions of the Raman effect and the TOD to the timing jitter. Variances of the soliton amplitude, frequency, and position fluctuations at the output of an amplifier, because of the spontaneous-emission noise added during the amplification process, have been derived earlier[16,18] and are given by

$$\sigma_A^2 = 2A_0n_{\mathrm{sp}}F(G)/N_s,$$
$$\sigma_\omega^2 = 2A_0n_{\mathrm{sp}}F(G)/(3N_s),$$
$$\sigma_q^2 = \pi^2n_{\mathrm{sp}}F(G)/(6A_0N_s), \quad (30)$$

where n_{sp} is the spontaneous-emission factor (set to 2), $F(G) = G - 1$ [for average solitons, $F(G) = (G - 1)^2/(G \ln G)$], the total gain $G = \exp(\alpha z_a)$ for each amplifier, and N_s is the average number of photons in each soliton before entering the DDF (for average solitons, N_s is the average number of photons in the fiber). Equation (29), with variances of the soliton parameters given by Eqs. (30), represents the total rms timing jitter and is valid for solitons as short as ~0.1 ps.

4. RESULTS AND DISCUSSION

In this section we evaluate the timing jitter by using Eq. (29) and compare the relative contributions of various physical mechanisms involved. The parameter values used correspond to a realistic soliton communication system designed to operate near 1.55 μm at bit rates in the range 20–100 GHz. The GVD coefficient β_2 varies exponentially along each fiber section and is quantified by the minimum and maximum values, related to each other as $\beta_2^{\max} = \beta_2^{\min}\exp(\alpha z_a)$, where $z_a = L_A/L_D$ and L_A is the amplifier spacing. The parameter N in Eq. (29) is $N = L_T/L_A$, where L_T is the total transmission distance. The numerical values of the other fiber parameters are TOD coefficient $\beta_3 = 0.07$ ps^3/km, Raman parameter $\tau_R = T_R/T_0$ with $T_R = 6$ fs, and fiber loss $\alpha = 0.22$ dB/km. The parameter T_0 is determined for a soliton of width T_s by use of $T_s \simeq 1.763T_0$, which sets the value of the normalized soliton amplitude A_0 to 1.

Figures 3 and 4 show, for several soliton widths in the range 1–40 ps, how fluctuations of the three soliton parameters (amplitude, frequency, and position) contribute to the total rms timing jitter as a function of transmission distance by choosing $\beta_2^{\min} = -0.1$ ps^2/km and $L_A = 80$ km. The solid curve represents the total timing jitter computed from Eq. (29), and the broken curves represent the timing jitter for each type of fluctuations if considered separately. For 40-ps-wide solitons [Fig. 3(a)] the timing jitter originates mostly from frequency fluctuations and is essentially of the Gordon–Haus type, except at distances, <800 km, for which the position fluctuations [direct effect of amplifiers noise on the soliton position, last term of Eq. (29)] dominate over frequency fluctuations. For 20-ps-

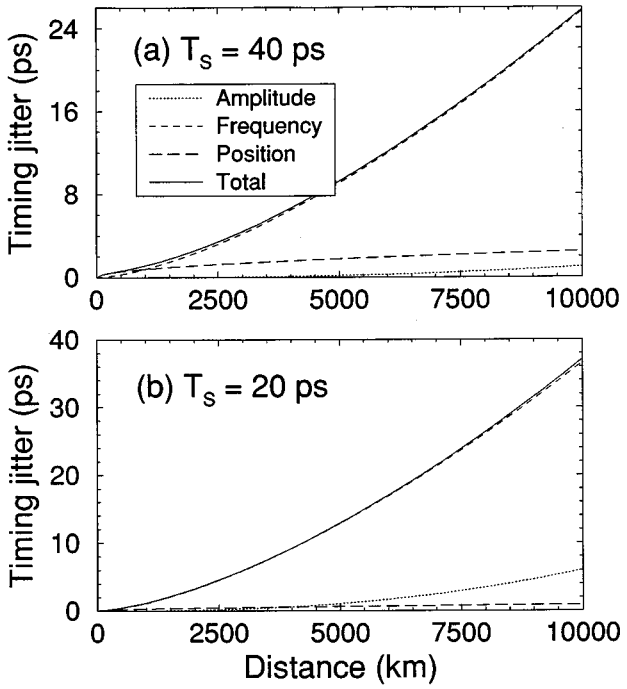

Fig. 3. Timing jitter as a function of transmission distance: (a) T_s = 40 ps; (b) T_s = 20 ps. Amplifier spacing is 80 km, and $\beta_2^{\min}$ is -0.1 ps^2/km. Timing jitter over 1000 km is dominated by frequency fluctuations for $T_s > 3$ ps and by amplitude fluctuations for $T_s < 1$ ps.

wide solitons, a typical width in the average-soliton regime, only frequency fluctuations contribute significantly [see Fig. 3(b)]. In fact, for transmission of solitons of width >10 ps over transoceanic distances (~10,000 km) the Gordon–Haus jitter dominates because the contributions of higher-order dispersive and nonlinear effects are small for such relatively broad solitons. Even though relatively quite small, the effect of higher-order terms (Raman and TOD) can be seen in Fig. 3 through the tiny contribution of amplitude fluctuations (dotted curve). When shorter solitons are used for transmission, the contribution of higher-order effects, especially the Raman effect, increases rapidly with transmission distance. For 3-ps or shorter solitons [Figs. 4(a) and 4(b)] the contribution of amplitude fluctuations to the timing jitter (mediated through the Raman effect) becomes so important that the total transmission distance is limited to only a few hundreds of kilometers in the absence of a soliton-control mechanism. Since the effect of amplitude fluctuations on the timing jitter increases more rapidly than that of frequency fluctuations [N^3 to N^7 versus N^3 to N^5 dependences in Eq. (29)], the former will dominate for long distances. Amplitude fluctuations start to dominate after 800 km for 3-ps solitons [Fig. 4(a)]. For a transoceanic distance of 10,000 km, one can calculate that amplitude fluctuations dominate for soliton widths <7 ps. For 1-ps solitons [Fig. 4(b)], amplitude fluctuations totally dominate the timing jitter even after 100 km. In fact, the Gordon–Haus jitter becomes negligible for 1-ps solitons after one amplifier spacing of 80 km.

The sharp transition between the dominance of amplitude and frequency fluctuations occurring near 3 ps can be understood by noting that the soliton self-frequency shift induced by the Raman effect depends on the soliton width as T_0^{-4}. Since the soliton width varies inversely with the soliton amplitude, the Raman effect converts amplitude fluctuations to frequency fluctuations, which are in turn transferred to temporal fluctuations through the GVD. Note that the exact value of soliton width at which amplitude fluctuations take over also depends on the numerical value of the parameter T_R. There is some uncertainty with respect to this parameter, and values in the range 2–10 fs have been used. We used T_R = 6 fs in this paper. The qualitative behavior, however, remains the same for other values of T_R.

From a practical standpoint the dependence of the timing jitter on the amplifier spacing is quite important. For DDF links the dependence is particularly strong since longer amplifier spacing increases the GVD at the input end for a given value of $\beta_2^{\min}$. The relative contributions of different physical mechanisms to the timing jitter as a function of the amplifier spacing are shown in Figs. 5(a) and 5(b) for 2-ps and 1-ps solitons, respectively, for propagation over 300 km. When only GVD is considered [first term of Eq. (22)], we recover the Gordon–Haus timing jitter (for DDF's). It is interesting to note that for moderate amplifier spacings (< 50 km) the timing jitter of a 2-ps soliton [Fig. 5(a)] has two components. The first one originates from the Gordon–Haus effect while a second component arises because of TOD. The latter effect [represented by the terms involving q_{TOD}^{A} in Eq. (29)] increases the timing jitter especially for small amplifier spacings and is further increased when combined with the Raman effect [because of the cross terms q_{C1} and q_{C2} appearing in Eqs. (29)].

For large amplifier spacings of more practical interest (>60 km) the Raman effect becomes increasingly of con-

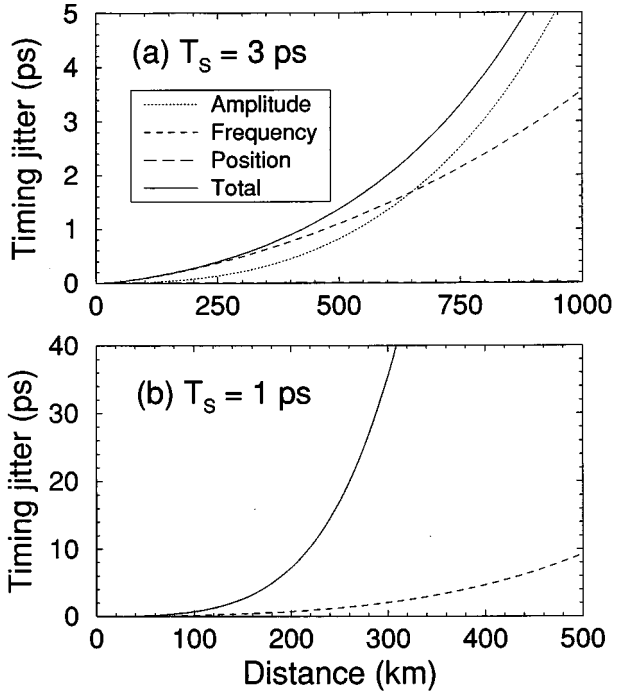

Fig. 4. Same as Fig. 3 except for (a) T_s = 3 ps and (b) T_s = 1 ps.

cern. This behavior can be understood by the rapid increase of the average GVD, $|\bar{\beta}_2|$, with the length of the DDF for a fixed $\beta_2^{\min}$ occurring at the fiber end. The average dispersion $\bar{\beta}_2$ is defined as $\bar{\beta}_2 = \int_0^{z_a} \beta_2(z)dz = \beta_2^{\min}[\exp(\alpha z_a) - 1]/(\alpha z_a)$. When TOD is included with the Raman effect, for large amplifier spacings, an increase in the timing jitter is observed in Fig. 5(a). This effect originates again from the cross terms q_{C1} and q_{C2} in Eqs. (29). Interestingly, if the sign of β_3 is inverted, as may be the case in dispersion-flattened fibers,[13] TOD can be used to reduce the timing jitter caused by the combined action of TOD and the Raman effect.

The relative contribution of TOD to the timing jitter increases as the soliton duration decreases. As seen in Fig. 5(b), the timing jitter of a 1-ps soliton under the same conditions as of Fig. 5(a) increases dramatically. Such behavior suggests that the control of TOD is of prime importance for reducing the timing jitter of communication systems making use of picosecond or subpicosecond solitons.

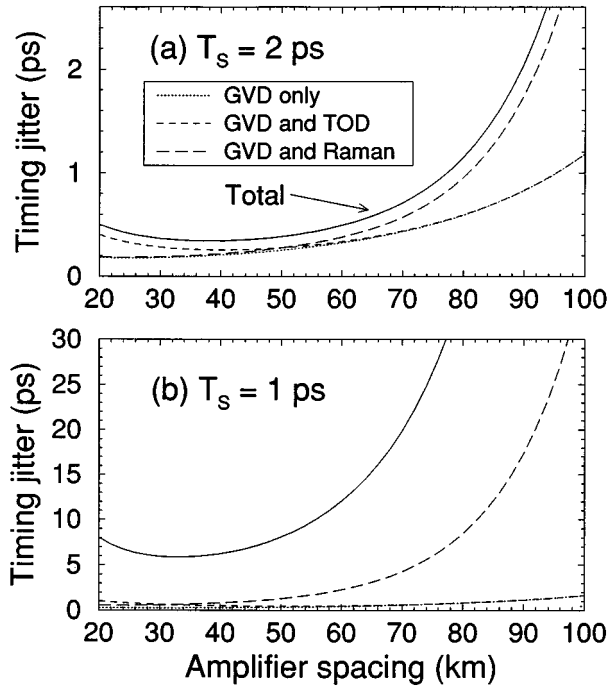

Fig. 5. Influence of GVD, TOD, and the Raman effect as a function of amplifier spacing for different fiber parameters when $\beta_2^{\min} = -0.1$ ps^2/km: (a) $T_s = 2$ ps; (b) $T_s = 1$ ps. The total distance of propagation is 300 km.

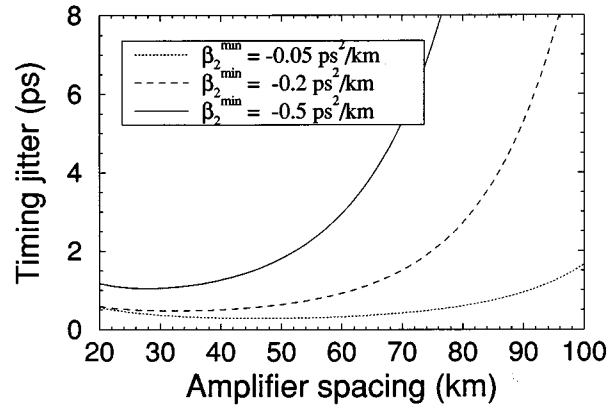

Fig. 6. Influence of the minimum dispersion $\beta_2^{\min}$ on the timing jitter as a function of amplifier spacing. Soliton width T_s is 2 ps, and the total distance of propagation is 300 km.

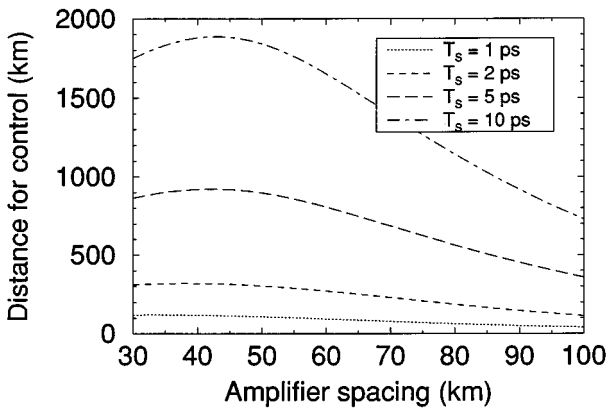

Fig. 7. Estimate of the soliton control distance as a function of amplifier spacing for different soliton widths in the range 1–10 ps. $\beta_2^{\min} = -0.1$ ps^2/km.

Since the average dispersion of a DDF depends strongly on the minimum dispersion $\beta_2^{\min}$ realizable at the fiber end, one should expect a strong dependence of the timing jitter on both $\beta_2^{\min}$ and amplifier spacing L_A. Figure 6 shows the total timing jitter as a function of the amplifier spacing for three values of $\beta_2^{\min}$. As $\beta_2^{\min}$ increases, $\beta_2^{\max}$ at the fiber input becomes quite large for long amplifier spacings. Indeed, amplifier spacings >60 km are possible only if $|\beta_2^{\min}| < 0.2$ ps^2/km. However, for $|\beta_2^{\min}| < 0.1$ ps^2/km, numerical simulations show that the TOD tends to enhance the timing jitter by introducing additional amplitude variations and dispersive waves that are not accounted for in the APT used in the derivation of Eq. (29). Two mechanisms are responsible for these additional amplitude fluctuations. First, dispersive waves beat with the soliton to induce periodic amplitude fluctuations. The second mechanism is related to the spectral variation of β_2 (owing to TOD) over the soliton spectrum, which translates into a temporal distortion of the soliton. The characterization of these effects on the timing jitter is beyond the scope of this paper as it requires either extensive numerical simulations or the use of the inverse scattering theory.

From a practical standpoint the jitter needs to be reduced through some form of soliton control. The question is how often such a control must be applied. We provide an estimate of the soliton-control distance by plotting in Fig. 7 the distance at which the rms timing jitter becomes 20% of the soliton width as a function of amplifier spacing for several solitons widths. As also observed experimentally,[19,20] broad solitons (>10 ps) require synchronous modulation on a scale of thousands of kilometers (or more frequent sliding-frequency filters). However, Fig. 7 shows that the use of short solitons will require soliton control at every amplifier section. The case of 1-ps solitons (dotted curve) suggests that not only an active form of control needs to be applied at each amplifier, but amplitude fluctuations that dominate in this regime also need to be controlled immediately after each

amplifier in order to reduce the timing jitter over the entire link. Optical bandpass filters may be a good candidate for this type of control.

5. CONCLUSION

We have derived, using adiabatic perturbation theory, an expression for the soliton trajectory and the timing jitter for transmission of ultrashort solitons in dispersion-tailored fibers. We have shown that, as the soliton width decreases, the nature of the timing jitter changes from a regime in which frequency fluctuations dominate (Gordon–Haus jitter) to a regime in which amplitude fluctuations dominate. For an amplifier spacing of 80 km and bit rates ~50 Gb/s the transition occurs for soliton widths of ~3 ps at a distance of ~500 km. The transition distance can be increased to transoceanic distances by use of wider solitons of width 7 ps. We included explicitly the contribution of third-order dispersion to the timing jitter and found that, while this contribution is quite small for solitons wider than ~3 ps, it becomes quite important for shorter solitons, especially for femtosecond solitons.

APPENDIX A: SOLITON TRAJECTORY IN THE PRESENCE OF FLUCTUATIONS

In this appendix we derive the expression [Eq. (28)] for the position fluctuation δq_N of an ultrashort soliton, at the end of a transmission line composed of N sections (see Fig. 1), resulting from fluctuations in soliton frequency, amplitude, and position induced by the noise added by N amplifiers.

Even though the expressions for the soliton position [Eq. (21)] and position fluctuation [Eq. (27)] established for a single section are useful to understand the effects of different parameters on the trajectory within one DDF, they cannot be easily generalized for a chain of amplifiers. Instead, one should reconsider the set of differential equations [Eqs. (15)–(17)] rewritten here in terms of the normalized amplitude A and distance z by using Eqs. (3) together with $A = Bp^{1/2}$:

$$\frac{dA}{dz} = -\frac{1}{2}\,\alpha A, \tag{31}$$

$$\frac{d\omega}{dz} = -\frac{8}{15}\,\tau_R \exp(\alpha z) A^4, \tag{32}$$

$$\frac{dq}{dz} = -\exp(-\alpha z)\omega + \delta_d[\exp(\alpha z)A^2 + 3\omega^2], \tag{33}$$

where a loss-matched dispersion profile $p(z) = \exp(-\alpha z)$ is used.

We start by using Eq. (31) to write the amplitude $A_p(z)$ of a soliton at a given position z $(0 < z < z_a)$ within the DDF of the pth section (see Fig. 1 of the text) of the transmission line:

$$A_p(z) = \exp(-\alpha z/2)(A_{p-1} + \delta A_p), \tag{34}$$

$$= \exp(-\alpha z/2)\left(A_0 + \sum_{i=1}^{p} \delta A_i\right), \tag{35}$$

where Eq. (35) is obtained by use of Eq. (34) recursively and $A_1 \equiv A_0 + \delta A_1$ with A_0 defined as the input soliton amplitude. Equation (35) merely states that amplitude fluctuations induced by all previous amplifiers should be added to the input amplitude A_0. Using Eqs. (32) and (35), one can write the soliton frequency $\omega_p(z)$ at a given point z within the pth DDF as

$$\omega_p(z) = -\frac{8}{15}\,\tau_R z_1(z) A_0^4 - \frac{32}{15}\,\tau_R z_1(z) A_0^3 \times \sum_{i=1}^{p} \delta A_i + \delta\omega_p + \omega_{p-1}(z), \tag{36}$$

$$= -\frac{8}{15}\,\tau_R z_1(z) \sum_{i=1}^{p} A_0^4 - \frac{32}{15}\,\tau_R z_1(z) A_0^3 \times \sum_{i=1}^{p}\sum_{j=1}^{i} \delta A_j + \sum_{i=1}^{p} \delta\omega_i\,, \tag{37}$$

where Eq. (37) is obtained by use of Eq. (36) recursively and only terms linear in δA_i are retained. Note that the frequency shift $\omega_{p-1}(z)$ at the end of the $(p-1)$th section had to be included because the soliton frequency at the end of the pth section is the sum of the frequency shift occurring over the pth section and the frequency shift of the soliton accumulated before entering the pth section.

We obtain the trajectory $q_p(z)$ of a soliton in the presence of small perturbations by using Eqs. (35) and (37) in Eq. (33) and integrating over z. The result is

$$\begin{aligned} q_p(z) = {} & q_R(z)\sum_{i=1}^{p} A_0^4 + q_{\mathrm{TOD}}^{A}(z) A_0^2 + q_{\mathrm{C1}}(z)\sum_{m=1}^{p}\sum_{n=1}^{p} A_0^8 \\ & + q_{\mathrm{GH}}(z)\sum_{i=1}^{p} \delta\omega_i + 4q_R(z)A_0^3\sum_{i=1}^{p}\sum_{j=1}^{i} \delta A_j \\ & + 2q_{\mathrm{TOD}}^{A}(z)A_0\sum_{i=1}^{p} \delta A_i \\ & + q_{\mathrm{C2}}(z)A_0^4\sum_{m=1}^{p}\sum_{i=1}^{p} \delta\omega_i \\ & + 8q_{\mathrm{C1}}(z)A_0^7\sum_{m=1}^{p}\sum_{i=1}^{p}\sum_{j=1}^{i} \delta A_j + \delta q_p + q_{p-1}(z). \end{aligned} \tag{38}$$

We obtain the soliton position $q_N \equiv q_N(z_a)$ at the end of a chain of N sections by first setting $z = z_a$ in Eq. (38), solving the recurrence relation to obtain q_p, and then allowing p to become N. The resulting expression is

$$q_N = q_R(z_a)\sum_{p=1}^{N}\sum_{i=1}^{p} A_0^4 + q_{\mathrm{TOD}}^{A}(z_a)\sum_{p=1}^{N} A_0^2 + q_{\mathrm{C1}}(z_a)\sum_{p=1}^{N}\sum_{m=1}^{p}\sum_{n=1}^{p} A_0^8 + q_{\mathrm{GH}}(z_a)\sum_{p=1}^{N}\sum_{i=1}^{p}\delta\omega_i + 4q_R(z_a)A_0^3\sum_{p=1}^{N}\sum_{i=1}^{p}\sum_{j=1}^{i}\delta A_j + 2q_{\mathrm{TOD}}^{A}(z_a)A_0\sum_{p=1}^{N}\sum_{i=1}^{p}\delta A_i + q_{\mathrm{C2}}(z_a)A_0^4\sum_{p=1}^{N}\sum_{m=1}^{p}\sum_{i=1}^{p}\delta\omega_i + 8q_{\mathrm{C1}}(z_a)A_0^7\sum_{p=1}^{N}\sum_{m=1}^{p}\sum_{i=1}^{p}\sum_{j=1}^{i}\delta A_j + \sum_{p=1}^{N}\delta q_p\,. \tag{39}$$

Equation (39) is a general expression for the trajectory of an ultrashort soliton for the communication system shown in Fig. 1. It includes the effects of amplitude and frequency fluctuations induced by the amplifier noise. For DDF's the trajectory q_N is obtained by use of the parameter values from Eqs. (22)–(25) while for constant-dispersion fibers the corresponding values are given by Eqs. (26). In absence of amplifier noise the soliton trajectory is given by the first three terms on the right side of Eq. (39). In such a case the first term represents the displacement due to the Raman effect only, the second the displacement due to TOD only, and the third-term, displacements due to the combined effect of TOD and the Raman effect. In the absence of any higher-order effects (Raman and TOD), the soliton displacement is zero, as it should be for an ideal soliton. Since the absence of fluctuations all solitons follow identical trajectories, only the relative displacement of a soliton from the average trajectory is important to determine the timing jitter. Such position displacement δq_N at the end of a transmission line is given by Eq. (39) with the first three terms on its right side removed. The result is Eq. (28), used in the text to evaluate the timing jitter.

ACKNOWLEDGMENTS

This work was supported by the Fonds pour la Formation de Chercheurs et l'Aide à la Recherche of the Québec government (Canada), the U.S. Army Research Office, and the National Science Foundation (grant PHY94-15583).

*E-mail, rjessiam@optics.rochester.edu; telephone, 716 275-6892; fax, 716 244-4936.

†E-mail, gpa@optics.rochester.edu; telephone, 716 275-4846; fax, 716 244-4936.

REFERENCES

1. L. F. Mollenauer and K. Smith, "Demonstration of soliton transmission over more than 4000 km in fiber with loss periodically compensated by Raman gain," Opt. Lett. **13**, 675–677 (1988).
2. A. Hasegawa and Y. Kodama, "Guiding-center soliton in optical fibers," Opt. Lett. **15**, 1443–1445 (1990).
3. J. P. Gordon and H. A. Haus, "Random walk of coherently amplified solitons in optical fibers," Opt. Lett. **11**, 665–667 (1986).
4. L. F. Mollenauer, J. P. Gordon, and S. G. Evangelides, "The sliding-frequency guiding filter: an improved form of soliton control," Opt. Lett. **17**, 1575–1577 (1992).
5. M. Nakazawa, E. Yamada, H. Kubota, and K. Suzuki, "10 Gb/s soliton transmission over one million kilometers," Electron. Lett. **27**, 1270–1271 (1991).
6. L. F. Mollenauer, S. G. Evangelides, and J. P. Gordon, "Wavelength division multiplexing with solitons in ultra long distance transmission using lumped amplifiers," J. Lightwave Technol. **9**, 362–367 (1991).
7. R. Vallée and R.-J. Essiambre, "Long distance soliton transmission with a nonlinear twin-core fiber," Opt. Lett. **19**, 2095–2097 (1994).
8. N. J. Smith and N. J. Doran, "Picosecond soliton propagation using nonlinear optical loop mirrors as intensity filters," Electron. Lett. **30**, 1084–1085 (1994).
9. R.-J. Essiambre and G. P. Agrawal, "Soliton communication beyond the average-soliton regime," J. Opt. Soc. Am. B **12**, 2420–2425 (1995).
10. R.-J. Essiambre and G. P. Agrawal, "Ultrahigh bit-rate soliton communication systems using dispersion-decreasing fibers and parametric amplifiers," Opt. Lett. **21**, 116–118 (1996), and references cited therein.
11. D. Wood, "Constraints on the bit rates in direct detection optical communication systems using linear and soliton pulses," J. Lightwave Technol. **8**, 1097–1106 (1990).
12. D.-M. Baboiu, D. Mihalache, and N.-C. Panoiu, "Combined influence of amplifier noise and intrapulse Raman scattering on the bit rate limit of optical fiber communication systems," Opt. Lett. **20**, 2282–2284 (1995).
13. G. P. Agrawal, *Nonlinear Fiber Optics*, 2nd ed. (Academic, Boston, Mass., 1995).
14. V. I. Karpman and E. M. Maslov, "Perturbation theory for solitons," Sov. Phys. JETP **46**, 281–291 (1977).
15. T. Georges, "Perturbation theory for the assessment of soliton control," Opt. Fiber Technol. **1**, 97–116 (1995).
16. T. Georges and F. Favre, "Modulation, filtering and initial phase control of interacting solitons," J. Opt. Soc. Am. B **10**, 1880–1889 (1993).
17. J. P. Gordon, "Theory of the soliton self-frequency shift," Opt. Lett. **11**, 662–664 (1986).
18. H. A. Haus and Y. Lai, "Quantum theory of soliton squeezing: a linearized approach," J. Opt. Soc. Am. B **7**, 386–392 (1990).
19. M. Nakazawa, K. Suzuki, H. Kubota, E. Yamada, and Y. Kimura, "Straight-line soliton data transmission at 20 Gbit/s beyond Gordon–Haus limit," Electron. Lett. **30**, 1331–1333 (1994).
20. K. Suzuki, E. Yamada, H. Kubota, and M. Nakazawa, "Optical soliton communication system using erbium-doped fiber amplifiers," Fiber Integrated Opt. **13**, 45–64 (1994).